Dynamical simulation of inelastic quantum transport

2007 J. Phys.: Condens. Matter 19 196201

(http://iopscience.iop.org/0953-8984/19/19/196201)

IOP PUBLISHING JOURNAL OF PHYSICS: CONDENSED MATTER

J. Phys.: Condens. Matter **19** (2007) 196201 (23pp) doi:10.1088/0953-8984/19/19/196201

Dynamical simulation of inelastic quantum transport

Eunan J McEniry[1], D R Bowler[2,3], Daniel Dundas[1], Andrew P Horsfield[4], Cristián G Sánchez[5] and Tchavdar N Todorov[1]

[1] Atomistic Simulation Centre, School of Mathematics and Physics, Queen's University of Belfast, Belfast BT7 1NN, UK
[2] Department of Physics and Astronomy, University College London, Gower Street, London WC1E 6BT, UK
[3] London Centre for Nanotechnology, 17–19 Gordon Street, London WC1H 0AH, UK
[4] Department of Materials, Imperial College London, South Kensington Campus, London SW7 2AZ, UK
[5] Unidad de Matemática y Física, Facultad de Ciencias Quimícas, INFIQC, Universidad Nacional de Córdoba, Ciudad Universitaria, 5000 Córdoba, Argentina

E-mail: e.mceniry@qub.ac.uk and t.todorov@qub.ac.uk

Received 23 February 2007
Published 18 April 2007
Online at stacks.iop.org/JPhysCM/19/196201

Abstract

A method for correlated quantum electron–ion dynamics is combined with a method for electronic open boundaries to simulate in real time the heating, and eventual equilibration at an elevated vibrational energy, of a quantum ion under current flow in an atomic wire, together with the response of the current to the ionic heating. The method can also be used to extract inelastic current–voltage corrections under steady-state conditions. However, in its present form the open-boundary method contains an approximation that limits the resolution of current–voltage features. The results of the simulations are tested against analytical results from scattering theory. Directions for the improvement of the method are summarized at the end.

(Some figures in this article are in colour only in the electronic version)

1. Introduction

Molecular dynamics (MD) simulations coupled with electronic transport calculations have found fruitful applications in the study of nanoscale conductors by helping to establish a connection between the electrical and mechanical properties of these systems [1]. Electronic and atomic motion in such simulations can be coupled together at a variety of levels. Early simulations treated mechanical and transport properties separately, for example by carrying out an MD simulation of a nanoscale contact using an empirical interatomic potential and placing the series of atomic geometries thus generated into a separate steady-state conductance calculation [2–5]. In more advanced studies, an *ab initio* MD simulation of the atomic structure

is combined with a conductance calculation that uses the self-consistent one-electron potential from the simulation [6–8]. Such simulations give insight into the effect of changes in the atomic structure and geometry, driven for instance by an external strain, on the conductance of a nanocontact but cannot address the reverse question: how the flow of current affects the actual interatomic forces.

That question can be addressed by computing the forces on atoms (or, fundamentally, on the ions or nuclei) from the actual steady-state current-carrying electronic structure in an atomic or molecular wire under bias [9–11]. The forces on atoms calculated in this way contain current-induced corrections due to the difference between the electronic structure under current and the ground-state electronic structure. Such calculations, therefore, can shed light onto the driving force for processes such as electromigration, in which current flow, together with thermal activation, can induce atomic rearrangements and a flow of atoms. This type of calculation, however, remains akin to Born–Oppenheimer dynamics, in that, for a given atomic geometry, electron–ion scattering is treated as purely elastic and the electronic subsystem is assumed to always remain in the steady state appropriate to the given ionic positions. It therefore cannot yet capture the inelastic scattering of electrons by atomic vibrations and the resultant exchange of energy between the two.

The next step in the dynamical simulation of atomic-scale conductors is to seek forms of MD in which both electrons and ions are treated dynamically under current flow in a way that captures simultaneously the departures from equilibrium in each subsystem, and the forces of interaction and the exchange of energy between them. The motivation behind this effort is to be able to simulate the current-driven dynamics of ions in real atomic-scale conductors and to model experimentally detectable phenomena, such as the heating of atomic vibrations by current-carrying electrons [12–14], the current–voltage (I–V) corrections arising from the inelastic scattering of electrons by nuclear vibrations [15], and the failure of a nanowire under high currents [16], as real-time, dynamical processes.

Ehrenfest dynamics is a form of non-adiabatic MD that has been combined with methods for electronic open boundaries (OB) to do time-dependent simulations of electron–nuclear dynamics under current [17, 18]. Ehrenfest dynamics, however, is a form of mean-field electron–ion dynamics, which does not give a full description of inelastic scattering. It can describe the excitation of electrons by energetic nuclei but suppresses the reverse process: the excitation of atomic vibrations by the non-radiative decay of excited electrons [19–21].

A recently proposed method for correlated electron–ion dynamics (CEID) reinstates the lowest-order corrections to Ehrenfest dynamics by an expansion of the electron–ion quantum Liouville equation in powers of correlated electron–ion fluctuations. This expansion was carried out to first order in reference [20] and was combined with electronic OB in [22]. The first-order expansion gives the power injected into atomic vibrations by excited electrons [20], but is unable to describe the response of the electrons to the resultant vibrational heating because of the absence of dynamical variables at that level of the expansion that keep track of the breathing of the ionic distribution due to inelastic scattering with electrons. When carried over to second order [21], the method does retain the variables needed to describe the exchange of energy between electrons and ions out of equilibrium and the response of electrons to the resultant variations in the ionic distribution.

In [21] the second-order CEID expansion was applied to current flow in finite systems to observe the onset of phonon excitation by current-carrying electrons. However, these finite-system simulations were restricted to short timescales and could not be used to see the eventual steady state and the behaviour of the system on the way there.

The present work removes this limitation by combining the second-order CEID expansion with electronic OB to enable electron–ion dynamical simulations under current over long

timescales. The method is used for a model simulation of the heating of a quantum ion in an atomic wire, from the onset of inelastic scattering to the eventual equilibration of the ion with the current at an appropriate elevated ionic vibrational energy, together with the accompanying response of the current to the changing scattering cross-section of the ion.

The electronic OB method used to generate and maintain current flow in the present paper is a re-formulation of the methods in [17, 22, 23]. As in those references, we work with the one-electron density matrix (DM). The choice of the DM, as opposed to electronic wavefunctions [24] or time-dependent Green's functions [25], is dictated by the method for CEID in [20, 21], which is formulated in terms of the DM and DM-like electron–ion correlation operators. The DM has the benefit that it allows a compact description of both the electronic wavefunctions and their occupancies.

The present OB method differs from those in [17, 22, 23] in the way in which the OB driving terms for a system between two electrodes are constructed and interpreted. In [17, 22, 23] a damping mechanism is introduced in the electrodes that continually drives the electronic DM therein towards a reference value. Different choices are possible for this reference value (and, in the case of CEID, for the electron–ion correlation operators) and for the relative strengths with which different subblocks of matrices are damped.

Here, this choice is restricted by invoking an explicit realization of the external battery that leads to an explicit expression for the OB terms for the reduced one-electron DM in the system connected to the battery. The driving terms explicitly contain the electronic energy distributions of the external reservoirs. This is important, because these distributions, together with the intrinsic properties of the conducting system, control the transport characteristics of the assembly. For time-independent Hamiltonians the method guarantees exact agreement with the conventional two-terminal Landauer formalism in well-defined limits.

For time-dependent Hamiltonians the OB terms for the DM are temporally non-local. To apply the OB method to dynamical electron–ion simulations, here we introduce an approximation that removes this temporal non-locality and makes the OB terms independent of the dynamical scattering of electrons in the system of interest. This approximation, however, introduces an energy broadening in the incoming electronic distributions, which limits the resolution of I–V features. Extensions beyond this approximation are a subject for future work.

The next two sections describe the OB method, first from a static and then from a time-dependent point of view. The method is then combined with CEID and is applied to the I–V spectrum of a quantum ion in a one-dimensional atomic wire, and to the heating and equilibration of the ion with the current-carrying electrons in real time, under different biases. The simulations are compared against analytical results from scattering theory for the present simple system, and against closed-system CEID simulations. Directions for future work are discussed at the end.

2. The multiple-probe battery: elastic steady state

We consider the system in figure 1. It consists of three finite, though possibly large, regions L, C and R. Label S will denote the LCR assembly as a whole. We use a discrete orthonormal real-space one-electron basis $\{|i\rangle\}$, such as a real-space grid or a tight-binding orbital basis. Each site (or orbital basis state) i in regions L and R is weakly coupled to an external probe, P_i, through a Hamiltonian matrix element γ_i. Each probe in isolation has a retarded and advanced surface Green's function $g^{\pm}_{P_i}(E)$ and a surface local density of states $d_{P_i}(E) = -\pi^{-1}\,\mathrm{Im}\,g^{+}_{P_i}(E)$.

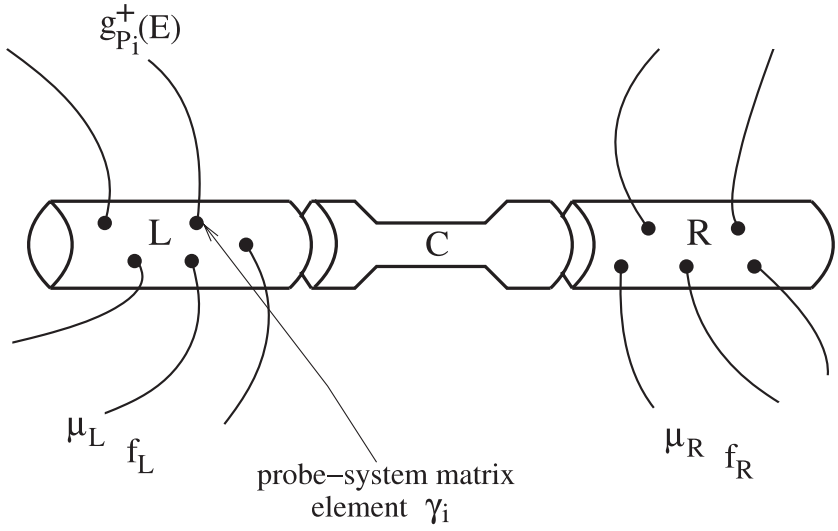

Figure 1. The $S = LCR$ system with multiple probes attached to regions L and R.

All probes attached to sites in $L(R)$ are maintained at an electrochemical potential $\mu_{L(R)}$, with a corresponding electronic Fermi–Dirac distribution $f_{L(R)}(E)$. A probe-specific electrochemical potential and electronic temperature may be introduced, but we will not do that here. Electrons are treated as non-interacting or as interacting through an effective mean-field one-electron potential. The benefits of the multiple-probe assembly are summarized at the end of this section and at the end of section 3.1.

The system S in the presence of the external probes is characterized by an electronic self-energy

$$\hat{\Sigma}^{\pm}(E) = \sum_{i\in L} |i\rangle\gamma_i^2 g^{\pm}_{P_i}(E)\langle i| + \sum_{i\in R} |i\rangle\gamma_i^2 g^{\pm}_{P_i}(E)\langle i| = \hat{\Sigma}^{\pm}_L(E) + \hat{\Sigma}^{\pm}_R(E). \tag{1}$$

If the components L, C and R are connected, a current flows in the system. Using, for example, the Lippmann–Schwinger equation for the wavefunctions of electrons incident on S from individual probes [26], the one-electron DM in S in the steady state may be written as

$$\hat{\rho}_S = \int_{-\infty}^{+\infty} \hat{G}^{+}_S(E)\hat{\Sigma}^{<}(E)\hat{G}^{-}_S(E)\,\mathrm{d}E \tag{2}$$

where[6]

$$\hat{G}^{\pm}_S(E) = [E\hat{1}_S - \hat{H}_{S_0} - \hat{\Sigma}^{\pm}(E)]^{-1} \tag{3}$$

$$\begin{aligned}\hat{\Sigma}^{<}(E) &= f_L(E)\sum_{i\in L} |i\rangle\gamma_i^2 d_{P_i}(E)\langle i| + f_R(E)\sum_{i\in R} |i\rangle\gamma_i^2 d_{P_i}(E)\langle i| \\ &= \frac{1}{2\pi\mathrm{i}}\, f_L(E)[\hat{\Sigma}^{-}_L(E) - \hat{\Sigma}^{+}_L(E)] + \frac{1}{2\pi\mathrm{i}}\, f_R(E)[\hat{\Sigma}^{-}_R(E) - \hat{\Sigma}^{+}_R(E)].\end{aligned} \tag{4}$$

Here

$$\hat{H}_{S_0} = \hat{H}_L + \hat{H}_{LC} + \hat{H}_{CL} + \hat{H}_C + \hat{H}_{CR} + \hat{H}_{RC} + \hat{H}_R \tag{5}$$

[6] The present notation occasionally departs from standard definitions; all quantities used are as defined in the text.

is the one-electron Hamiltonian in S,[7] which for the moment is treated as time-independent and which may have been self-consistently calculated. Here, and below,

$$\hat{1}_M = \sum_{i \in M} |i\rangle\langle i| \tag{6}$$

denotes the identity operator in region M. We will also use the notation

$$\hat{A}_{MN} = \hat{1}_M \hat{A} \hat{1}_N, \qquad \hat{A}_M \equiv \hat{A}_{MM} \tag{7}$$

for a one-electron operator $\hat{A}$.

By use of the Dyson equation, the DM in region C may be written as

$$\hat{\rho}_C = \int_{-\infty}^{+\infty} \hat{G}_C^+(E)\hat{\sigma}^<(E)\hat{G}_C^-(E)\,\mathrm{d}E \tag{8}$$

$$\hat{\sigma}^<(E) = \hat{H}_{CL} f_L(E) \hat{d}_L(E) \hat{H}_{LC} + \hat{H}_{CR} f_R(E) \hat{d}_R(E) \hat{H}_{RC} \tag{9}$$

$$\hat{G}_C^\pm(E) = [E\hat{1}_C - \hat{H}_C - \hat{\sigma}^\pm(E)]^{-1} \tag{10}$$

$$\hat{\sigma}^\pm(E) = \hat{H}_{CL}\hat{g}_L^\pm(E)\hat{H}_{LC} + \hat{H}_{CR}\hat{g}_R^\pm(E)\hat{H}_{RC} \tag{11}$$

where

$$\hat{g}_{L(R)}^\pm(E) = [E\hat{1}_{L(R)} - \hat{H}_{L(R)} - \hat{\Sigma}_{L(R)}^\pm(E)]^{-1}, \qquad \hat{d}_{L(R)}(E) = \frac{1}{2\pi\mathrm{i}}[\hat{g}_{L(R)}^-(E) - \hat{g}_{L(R)}^+(E)] \tag{12}$$

are the retarded and advanced Green's functions and density of states operator for region $L(R)$ coupled to its probes but not coupled to C.

The effect of the multiple probes is to smear out the discrete energy levels of the electrodes L and R, turning these regions into metals with a continuous density of states. If L and R are long enough and the coupling to the probes is weak enough, local matrix elements of $\hat{g}_{L(R)}^\pm(E)$ in the real-space basis may be expected to tend to those for semi-infinite electrodes. Then the steady-state electronic structure in C given by equations (8)–(12) becomes the same as what we would have written down in the conventional two-terminal setup, in which C is coupled to two semi-infinite metallic electrodes injecting electrons into C with electrochemical potentials μ_L and μ_R. Therefore, in the limit of long electrodes and weak probe–electrode coupling, we expect the multiple-probe assembly in figure 1 to produce the same steady-state electronic structure in region C as that in the two-terminal Landauer picture.

The above argument simplifies if we make the probe–system coupling the same for all probes, $\gamma_i = \gamma$, and the probe surface density of states an energy-independent constant (thus assuming the wideband limit in the probes), $d_{P_i}(E) = d$, $g_{P_i}^+(E) = -\pi\mathrm{i}d$. Then equations (1), (3) and (4) become

$$\hat{\Sigma}^+ = \hat{\Sigma}_L^+ + \hat{\Sigma}_R^+ = -\mathrm{i}\frac{\Gamma}{2}\hat{1}_L - \mathrm{i}\frac{\Gamma}{2}\hat{1}_R, \qquad \hat{\Sigma}^- = \hat{\Sigma}^{+\dagger} \tag{13}$$

$$\hat{G}_S^\pm(E) = (E\hat{1}_S - \hat{H}_{S_0} - \hat{\Sigma}^\pm)^{-1} \tag{14}$$

$$\hat{\Sigma}^<(E) = \frac{\Gamma}{2\pi} f_L(E)\,\hat{1}_L + \frac{\Gamma}{2\pi} f_R(E)\,\hat{1}_R \tag{15}$$

$$\Gamma = 2\pi\gamma^2 d \tag{16}$$

with $\hat{g}_{L(R)}^\pm(E) = (E\hat{1}_{L(R)} - \hat{H}_{L(R)} \pm \mathrm{i}\hat{1}_{L(R)}\Gamma/2)^{-1}$. Consider an individual local positional matrix element of $\hat{g}_{L(R)}^\pm(E)$, $(g_{L(R)}^\pm)_{ij}(E)$, such as one involving sites i, j coupled to C, and compare it with the corresponding matrix element, $(g_{L(R)}^{\infty\pm})_{ij}(E)$, of the Green's function

[7] The notation $\hat{H}_S = \hat{H}_S(t)$ is reserved for time-dependent Hamiltonians.

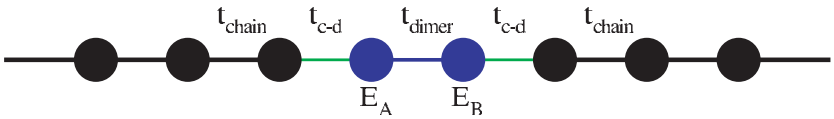

Figure 2. A resonant dimer in an atomic chain.

$\hat{g}^{\infty\pm}_{L(R)}(E) = (E\hat{1}^{\infty}_{L(R)} - \hat{H}^{\infty}_{L(R)} \pm \mathrm{i}\hat{1}^{\infty}_{L(R)}\epsilon)^{-1}$, $\epsilon \to 0^{+}$, for a semi-infinite lead. We can make the former an arbitrarily good approximation to the latter by making the finite lead longer and Γ smaller, while keeping Γ much larger than the energy-level spacing in the finite lead. In the limit, Γ takes over the role of ϵ, $(g^{\pm}_{L(R)})_{ij}(E) \to (g^{\infty\pm}_{L(R)})_{ij}(E)$, and the steady-state current-carrying DM in C in the multiple-probe case becomes the same as that in the two-terminal Landauer steady state with semi-infinite electrodes.

In practical terms, we expect agreement with the two-terminal Landauer steady state provided Γ is smaller than the energy scale, ϵ_{F}, of any relevant variations in the electronic structure of a truly semi-infinite lead near the Fermi level, and provided Γ is larger than the energy-level spacing in the finite leads in figure 1,

$$\frac{\pi\hbar v_{\mathrm{F}}}{l} < \Gamma < \epsilon_{\mathrm{F}} \tag{17}$$

where v_{F} is the electron Fermi velocity and l is the length of the finite lead.

This agreement is illustrated for a resonant dimer between two 1d electrodes (figure 2). In the multiple-probe realization of the system, each electrode is an atomic chain of length N_L atoms. The device region C consists of $N_D/2$ chain atoms on each side of the dimer. We use a nearest-neighbour single-orbital orthogonal tight-binding model with a hopping integral t_{chain} everywhere, except the lead-dimer hopping integral, $t_{\mathrm{c-d}}$, and the intradimer hopping integral, t_{dimer}. The onsite energies on all atoms outside the dimer are zero and those of the two dimer atoms are E_A and E_B. The bias V is applied symmetrically across the middle of the energy band, $\mu_{L(R)} = \pm eV/2$. The differential conductance $G(V) = \mathrm{d}I/\mathrm{d}V$, where I is the steady-state current in region C, for the multiple-probe assembly is compared with the two-terminal Landauer differential conductance in figures 3 and 4. The oscillations in the multiple-probe conductance originate from the finite energy-level spacing in the electrodes. The oscillations disappear as the electrode length is increased for a given Γ, or as Γ is increased for a given electrode length, leaving behind a good approximation to the two-terminal conductance.

To summarize, imposing the wideband limit directly in the electrodes (L, R) adjoining the device region (C) would in general be a restrictive approximation. However, in the case of the multiple-probe assembly, imposing the wideband limit in the external probes (and not directly in the electrodes) is a benign measure that generates, in a controlled way, arbitrarily good approximations to the two-terminal steady state (in region C) that would be calculated for semi-infinite leads with the correct electronic structure, appropriate to those leads.

3. Time-dependent formalism

We now use the multiple-probe assembly from the previous section to obtain effective electron injection and extraction terms for the one-electron DM in system S in the presence of dynamical scattering in region C. First we give a general derivation. Then we introduce an approximation that will be used for the simulations later. The present discussion is restricted to a time-independent Hamiltonian, $\hat{H}_P$, in the external probes, where P denotes the set of probes.

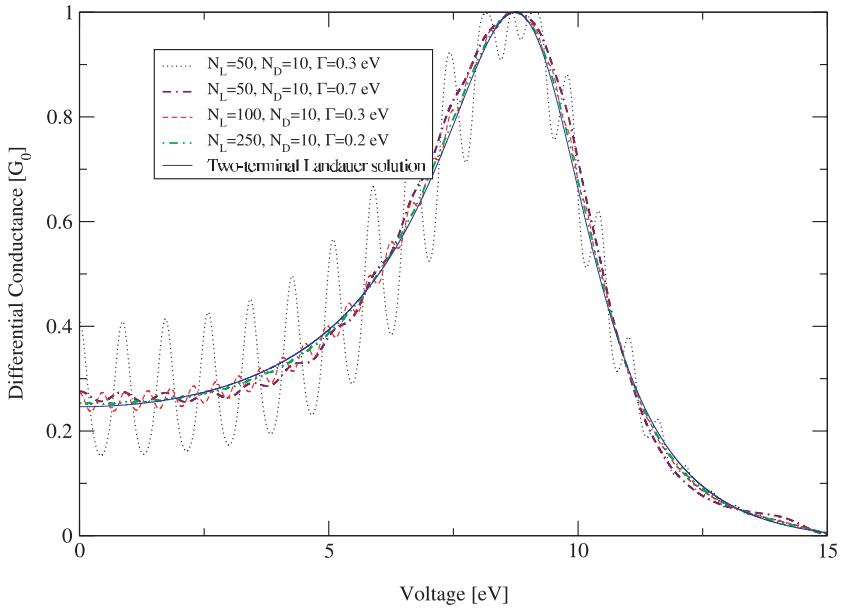

Figure 3. Differential conductance, in units of $G_0 = 2e^2/h$, for the system in figure 2, with $t_{\text{chain}} = -3.88$ eV, $t_{\text{c-d}} = -2$ eV, $t_{\text{dimer}} = -3.88$ eV, $E_A = E_B = 0$ eV. The bandwidth in the leads is $4t_{\text{chain}}$. The solid line is the two-terminal Landauer solution.

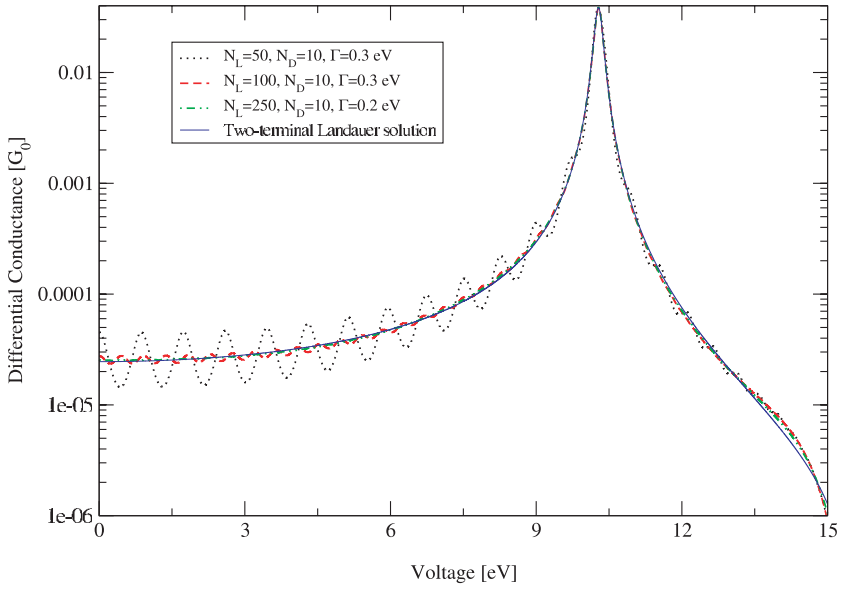

Figure 4. Differential conductance, in units of $G_0 = 2e^2/h$, for the system in figure 2, with $t_{\text{chain}} = -3.88$ eV, $t_{\text{c-d}} = -0.5$ eV, $t_{\text{dimer}} = -1$ eV, $E_A = 5$ eV, $E_B = -5$ eV. Note the logarithmic axis for the conductance.

3.1. General result

Let

$$\hat{H}(t) = \hat{H}_S(t) + \hat{H}_{SP}(t) + \hat{H}_{PS}(t) + \hat{H}_P \tag{18}$$

be an effective one-electron Hamiltonian for the combined system in figure 1. The SP couplings $H_{SP}(t) = \hat{H}^{\dagger}_{PS}(t)$ have been allowed to be time-dependent. The time dependence of the Hamiltonian in S, $\hat{H}_S(t)$, may come from a time-dependent external field acting in S, from some other dynamical scattering potential in S, or from temporal variations in the one-electron DM in S in a time-dependent density-functional (TDDFT) calculation[8]. We adopt the initial conditions that are frequently used in transport calculations based on the non-equilibrium Green's function (NEGF) method [27] or on scattering theory [26],

$$\hat{\rho}_P(0) = \hat{\rho}_{P_{\mathrm{eql}}} = \sum_{i\in L,R} \int_{-\infty}^{+\infty} f_{P_i}(E)\hat{d}_{P_i}(E)\,\mathrm{d}E, \qquad \hat{\rho}_{SP}(0) = \hat{\rho}_{PS}(0) = 0 \tag{19}$$

where $\hat{d}_{P_i}(E)$ is the density of states operator for probe P_i in isolation, and $\hat{\rho}_{P_{\mathrm{eql}}}$ is the equilibrium density matrix for the probes in isolation, with $f_{P_i}(E) = f_{L(R)}(E)$, $i \in L(R)$.[9] The wideband limit in the external probes has not been introduced at this stage.

The global one-electron DM $\hat{\rho}(t)$, for the SP system as a whole, evolves according to

$$\mathrm{i}\hbar\,\dot{\hat{\rho}}(t) = [\hat{H}(t), \hat{\rho}(t)]. \tag{20}$$

For the DM in S this gives [17]

$$\mathrm{i}\hbar\,\dot{\hat{\rho}}_S(t) = [\hat{H}_S(t), \hat{\rho}_S(t)] + \hat{H}_{SP}(t)\hat{\rho}_{PS}(t) - \hat{\rho}_{SP}(t)\hat{H}_{PS}(t). \tag{21}$$

The terms after the commutator are the OB driving terms for S that we wish to find. The solution to (20) is

$$\hat{\rho}(t) = \hat{W}(t,0)\hat{\rho}(0)\hat{W}^{\dagger}(t,0) \tag{22}$$

where the propagator $\hat{W}(t,\tau)$ for the combined SP system obeys

$$\mathrm{i}\hbar\,\frac{\partial \hat{W}(t,\tau)}{\partial t} = \hat{H}(t)\hat{W}(t,\tau), \qquad \hat{W}(\tau,\tau) = \hat{1} = \hat{1}_S + \hat{1}_P. \tag{23}$$

Let $\hat{H}_0(t) = \hat{H}_S(t) + \hat{H}_P$, $\hat{V}(t) = \hat{H}_{SP}(t) + \hat{H}_{PS}(t)$ and

$$\hat{U}_P(t,\tau) = \mathrm{e}^{-\mathrm{i}\hat{H}_P(t-\tau)/\hbar} \tag{24}$$

$$\mathrm{i}\hbar\,\frac{\partial \hat{U}_S(t,\tau)}{\partial t} = \hat{H}_S(t)\hat{U}_S(t,\tau), \qquad \hat{U}_S(\tau,\tau) = \hat{1}_S \tag{25}$$

$$\mathrm{i}\hbar\,\frac{\partial \hat{U}(t,\tau)}{\partial t} = \hat{H}_0(t)\hat{U}(t,\tau), \qquad \hat{U}(\tau,\tau) = \hat{1}. \tag{26}$$

Then

$$\hat{W}(t,\tau) = \hat{U}(t,\tau) + \frac{1}{\mathrm{i}\hbar}\int_{\tau}^{t} \hat{U}(t,\tau')\hat{V}(\tau')\hat{W}(\tau',\tau)\,\mathrm{d}\tau' \tag{27}$$

$$= \hat{U}(t,\tau) + \frac{1}{\mathrm{i}\hbar}\int_{\tau}^{t} \hat{W}(t,\tau')\hat{V}(\tau')\hat{U}(\tau',\tau)\,\mathrm{d}\tau' \tag{28}$$

$$\hat{W}^{\dagger}(t,\tau) = \hat{U}^{\dagger}(t,\tau) - \frac{1}{\mathrm{i}\hbar}\int_{\tau}^{t} \hat{W}^{\dagger}(\tau',\tau)\hat{V}(\tau')\hat{U}^{\dagger}(t,\tau')\,\mathrm{d}\tau'. \tag{29}$$

Define

$$\hat{\rho}(t,\tau) = \hat{W}(t,0)\hat{\rho}(0)\hat{W}^{\dagger}(\tau,0), \qquad \hat{\rho}(t) \equiv \hat{\rho}(t,t). \tag{30}$$

[8] We note, however, the care that must be taken in combining partitioned Hamiltonians of the above form with TDDFT discussed in [24].

[9] Alternative initial conditions are discussed in [24].

From (22) and (29),

$$\hat{\rho}_{SP}(t) = \hat{W}_{SP}(t,0)\hat{\rho}_P(0)\hat{U}_P^\dagger(t,0) - \frac{1}{\mathrm{i}\hbar}\int_0^t \hat{\rho}_S(t,\tau)\hat{H}_{SP}(\tau)\hat{U}_P^\dagger(t,\tau)\,\mathrm{d}\tau. \tag{31}$$

Using (28),

$$\begin{aligned}\hat{\rho}_{SP}(t)\hat{H}_{PS}(t) = {} & \frac{1}{\mathrm{i}\hbar}\int_0^t \hat{W}_S(t,\tau)\hat{H}_{SP}(\tau)\hat{U}_P(\tau,0)\hat{\rho}_P(0)\hat{U}_P^\dagger(t,0)\hat{H}_{PS}(t)\,\mathrm{d}\tau \\ & - \frac{1}{\mathrm{i}\hbar}\int_0^t \hat{\rho}_S(t,\tau)\hat{H}_{SP}(\tau)\hat{U}_P^\dagger(t,\tau)\hat{H}_{PS}(t)\,\mathrm{d}\tau\end{aligned} \tag{32}$$

where, from (27), the effective propagator in S, $\hat{W}_S(t,\tau)$, satisfies

$$\hat{W}_S(t,\tau) = \hat{U}_S(t,\tau) + \frac{1}{(\mathrm{i}\hbar)^2}\int_\tau^t \mathrm{d}\tau' \int_\tau^{\tau'} \mathrm{d}\tau''\, \hat{U}_S(t,\tau')\hat{H}_{SP}(\tau')\hat{U}_P(\tau',\tau'')\hat{H}_{PS}(\tau'')\hat{W}_S(\tau'',\tau). \tag{33}$$

Now we impose the wideband limit in the external probes P. This enables us to benefit from the great simplifications that this limit affords [25], while retaining the confidence that, as argued in the previous section, in the special case of the multiple-probe assembly this limit produces a controlled approximation to the conventional two-terminal transport problem. In the wideband limit, where all probes have an energy-independent surface local density of states d,

$$\begin{aligned}\hat{H}_{SP}(\tau)\hat{U}_P^\dagger(t,\tau)\hat{H}_{PS}(t) &= \hat{H}_{SP}(\tau)\int_{-\infty}^{+\infty} \mathrm{d}E\, \hat{d}_P(E)\,\mathrm{e}^{\mathrm{i}E(t-\tau)/\hbar}\,\hat{H}_{PS}(t) \\ &= 2\mathrm{i}\hbar\,\hat{\Sigma}^+(t)\,\delta(t-\tau) = -2\mathrm{i}\hbar\,\hat{\Sigma}^-(t)\,\delta(t-\tau)\end{aligned} \tag{34}$$

where $\hat{\Sigma}^+(t) = -\mathrm{i}\Gamma(t)\,(\hat{1}_L+\hat{1}_R)/2 = \hat{\Sigma}^{-\dagger}(t)$ with $\Gamma(t) = 2\pi\gamma^2(t)d$. Above, $\{|P\rangle\}$ and $\{E_P\}$ are the eigenstates and eigenvalues of the probe Hamiltonian $\hat{H}_P$, $\hat{d}_P(E) = \sum_{i\in L,R}\hat{d}_{P_i}(E) = \sum_P |P\rangle\delta(E-E_P)\langle P|$ is the probe density of states operator, and we have introduced the same conditions as in the previous section, namely that each probe couples to only one site in L or in R, with a matrix element $\gamma(t)$ (which now is allowed to be time-dependent) common to all probes.

Then (32), together with (19) and (21), gives the OB equation of motion for the DM in S

$$\begin{aligned}\mathrm{i}\hbar\,\dot{\hat{\rho}}_S(t) = {} & [\hat{H}_S(t),\hat{\rho}_S(t)] - \left(\hat{\rho}_S(t)\hat{\Sigma}^-(t) - \mathrm{h.c.}\right) \\ & - \left(\frac{1}{\mathrm{i}\hbar}\int_0^t \mathrm{d}\tau \int_{-\infty}^{+\infty} \mathrm{d}E\,\mathrm{e}^{\mathrm{i}E(t-\tau)/\hbar}\hat{W}_S(t,\tau)\,\hat{\Sigma}^<_{\tau t}(E) - \mathrm{h.c.}\right)\end{aligned} \tag{35}$$

where $\hat{\Sigma}^<_{\tau t}(E) = (2\pi)^{-1}\,\mathrm{sgn}[\gamma(\tau)]\mathrm{sgn}[\gamma(t)]\,\sqrt{\Gamma(\tau)\Gamma(t)}\,[f_L(E)\hat{1}_L + f_R(E)\hat{1}_R]$. For time-independent couplings, $\hat{\Sigma}^<_{\tau t}(E) = \hat{\Sigma}^<(E)$ from (15). Above, the integral in the second term in (32) has collected a factor of $1/2$ from the upper limit for τ which lies half way through the delta function, introduced by (34). The terms after the commutator in the first line of (35) are the effective extraction terms, responsible for the loss of electrons to the external probes. The terms in the second line are the injection terms into S. The OB terms operate only in S and involve only the instantaneous DM therein. The propagator in S, $\hat{W}_S(t,\tau)$, obeys

$$\mathrm{i}\hbar\,\frac{\partial\hat{W}_S(t,\tau)}{\partial t} = [\hat{H}_S(t) + \hat{\Sigma}^+(t)]\hat{W}_S(t,\tau), \qquad \hat{W}_S(\tau,\tau) = \hat{1}_S \tag{36}$$

$$\hat{W}_S(t,\tau) = \hat{U}_S(t,\tau) + \frac{1}{\mathrm{i}\hbar}\int_\tau^t \hat{U}_S(t,\tau')\hat{\Sigma}^+(\tau')\hat{W}_S(\tau',\tau)\,\mathrm{d}\tau'. \tag{37}$$

For a time-independent $\hat{H}_S = \hat{H}_{S_0}$ and time-independent SP coupling, $\hat{W}_S(t,\tau) = \mathrm{e}^{-\mathrm{i}(\hat{H}_{S_0}+\hat{\Sigma}^+)(t-\tau)/\hbar}$, and in the limit $t \to +\infty$ (35) becomes

$$\mathrm{i}\hbar\,\dot{\hat{\rho}}_S(t) = [\hat{H}_{S_0}, \hat{\rho}_S(t)] + \hat{\Sigma}^+\hat{\rho}_S(t) - \hat{\rho}_S(t)\hat{\Sigma}^- + \int_{-\infty}^{+\infty} [\hat{\Sigma}^<(E)\hat{G}_S^-(E) - \hat{G}_S^+(E)\hat{\Sigma}^<(E)]\,\mathrm{d}E \tag{38}$$

with $\hat{\Sigma}^\pm$, $\hat{G}_S^\pm(E)$ and $\hat{\Sigma}^<(E)$ given by equations (13), (14) and (15). Equation (2) is a steady-state solution to (38). Therefore, as may be expected, the time-dependent formalism returns the steady state given by stationary scattering theory.

To summarize the motivation for introducing the multiple-probe assembly in figure 1: (i) it enables the introduction of the wideband limit in P while retaining a controllable connection with the conventional two-terminal setup; (ii) this enables the OB driving terms in S to be expressed solely in terms of the instantaneous DM in S (without the wideband limit in the external probes, the second term in (32) retains the two-time quantity $\hat{\rho}_S(t,\tau)$); (iii) from a practical point of view, figure 1 removes the need for the usual computation of energy-dependent surface Green's functions that arises in the conventional two-terminal setup.

3.2. Approximate result

Our purpose now is to replace the injection terms in the second line of equation (35) by approximate injection terms that are temporally local and are independent of any dynamical scattering of electrons in region C. This approximation gains tractability, but also introduces a key limitation, discussed below.

The key approximation is to introduce a dephasing factor, $\mathrm{e}^{-(t-\tau)/\tau_\Delta}$, in the injection terms in the second line of (35), so that they now read

$$-\left(\frac{1}{\mathrm{i}\hbar}\int_0^t \mathrm{d}\tau \int_{-\infty}^{+\infty} \mathrm{d}E\,\mathrm{e}^{\mathrm{i}E(t-\tau)/\hbar}\mathrm{e}^{-(t-\tau)/\tau_\Delta}\hat{W}_S(t,\tau)\Sigma^<(E) - \mathrm{h.c.}\right) \tag{39}$$

where for simplicity we assume that the coupling $\Gamma(t)$ has been switched on over some early period to a constant value Γ, with t lying τ_Δ or more beyond that early period, and have replaced $\Gamma(t)$ and $\Gamma(\tau)$ by Γ. The time τ_Δ corresponds to an energy scale $\Delta = \hbar/\tau_\Delta$.

We can think of the relaxation time τ_Δ in two ways. First, it may describe a generic dephasing mechanism that restricts the duration of coherent propagation of signals between P and S. A further discussion of the introduction of decoherence factors is given in [25]. Second, for $t > 0, b > 0$,

$$\begin{aligned} &\int_{-b}^{0} \mathrm{e}^{\mathrm{i}\omega t}\,\mathrm{e}^{-t/\tau_\Delta}\,\mathrm{d}\omega = \int_{-\infty}^{+\infty} \mathrm{e}^{\mathrm{i}\omega t}\,\tilde{f}(\omega)\,\mathrm{d}\omega, \\ &\tilde{f}(\omega) = \frac{1}{\pi}\left(\tan^{-1}[(b+\omega)\tau_\Delta] - \tan^{-1}(\omega\tau_\Delta)\right). \end{aligned} \tag{40}$$

In the limit $b \to +\infty$, $\tilde{f}(\omega) \to (1/2 - \pi^{-1}\tan^{-1}(\omega\tau_\Delta))$. Therefore, the introduction of the dephasing factor $\mathrm{e}^{-(t-\tau)/\tau_\Delta}$ in (39) is equivalent to replacing the step-like Fermi–Dirac distributions of the probes $f_{L(R)}(E)$ (for simplicity, we consider the case of zero electronic temperature) in $\hat{\Sigma}^<(E)$ by the fictitious distributions $\tilde{f}_{L(R)}(E) = 1/2 - \pi^{-1}\tan^{-1}[(E - \mu_{L(R)})/\Delta]$. $\tilde{f}_{L(R)}(E)$ mimics $f_{L(R)}(E)$ in that $\tilde{f}_{L(R)}(-\infty) = 1$, $\tilde{f}_{L(R)}(\mu_{L(R)}) = 1/2$, $\tilde{f}_{L(R)}(+\infty) = 0$, but is broadened by 2Δ. The essential consequence of (39), therefore, is that electrons now arrive in S with fictitious energy distributions that have the same electrochemical potentials as the original distributions but contain the additional broadening. This places a corresponding restriction on the resolution of I–V spectral features. However, we can now

obtain temporally local injection terms, independent of the electron dynamics in region C, as follows.

Suppose that the Hamiltonian in S is composed of a time-independent Hamiltonian $\hat{H}_{S_0}$ together with a time-dependent scattering potential $\hat{v}(t)$ that operates solely in some subregion in the interior of region C, $\hat{H}_S(t) = \hat{H}_{S_0} + \hat{v}(t)$. Writing $\hat{W}_S(t,\tau) = \hat{W}_{S_0}(t,\tau) + (\mathrm{i}\hbar)^{-1}\int_\tau^t \hat{W}_S(t,\tau')\hat{v}(\tau')\hat{W}_{S_0}(\tau',\tau)\,\mathrm{d}\tau'$, where $\hat{W}_{S_0}(t,\tau) = \mathrm{e}^{-\mathrm{i}(\hat{H}_{S_0}+\hat{\Sigma}^+)(t-\tau)/\hbar}$ is the propagator in S in the presence of the probes and in the absence of $\hat{v}$, the first term in (39) becomes

$$\begin{aligned} &-\frac{1}{\mathrm{i}\hbar}\int_0^t \mathrm{d}\tau \int_{-\infty}^{+\infty} \mathrm{d}E\, \mathrm{e}^{\mathrm{i}E(t-\tau)/\hbar}\mathrm{e}^{-(t-\tau)/\tau_\Delta}\hat{W}_{S_0}(t,\tau)\Sigma^<(E) \\ &-\frac{1}{(\mathrm{i}\hbar)^2}\int_0^t \mathrm{d}\tau\int_\tau^t \mathrm{d}\tau' \int_{-\infty}^{+\infty} \mathrm{d}E\, \mathrm{e}^{\mathrm{i}E(t-\tau)/\hbar}\mathrm{e}^{-(t-\tau)/\tau_\Delta}\hat{W}_S(t,\tau')\hat{v}(\tau')\hat{W}_{S_0}(\tau',\tau)\Sigma^<(E). \end{aligned} \tag{41}$$

The product $\hat{v}(\tau')\hat{W}_{S_0}(\tau',\tau)\hat{\Sigma}^<(E)$ in the second term contains the amplitude for the transmission of a signal from a point in L, R (where the SP coupling operates) to the interior of C (where $\hat{v}$ operates), over a time $(\tau'-\tau)$. Because of the limits of integration $(\tau'-\tau) \leqslant (t-\tau)$. The real exponential, on the other hand, is significant only over $(t-\tau) < \tau_\Delta$. Therefore, provided the distance between L, R and the interior of C is greater than $v_\mathrm{e}\tau_\Delta$, where v_e is a typical electron group velocity, signals from L, R cannot reach the scattering potential $\hat{v}$ in the time $(\tau'-\tau)$ and the second term in (41) does not contribute. The injection of electrons into L, R has thus effectively been decoupled from their subsequent scattering in C. The origin of this decoupling is seen in physical terms if we think of the dephasing factor in (39) as a restriction, τ_Δ, on the duration of coherent propagation between S and P: if C is long enough, electrons that are being injected into L, R do not reach far enough into S, over this restricted duration, to be aware of what awaits them in C, and the injection process is governed chiefly by $\hat{H}_{S_0}$ (together with the SP coupling).

For times t an amount τ_Δ or more beyond the initial application of the SP coupling, from the first term in (41) we now obtain the OB equation of motion

$$\begin{aligned} \mathrm{i}\hbar\,\dot{\hat{\rho}}_S(t) &= [\hat{H}_S(t), \hat{\rho}_S(t)] + \hat{\Sigma}^+\hat{\rho}_S(t) - \hat{\rho}_S(t)\hat{\Sigma}^- \\ &\quad + \int_{-\infty}^{+\infty} [\hat{\Sigma}^<(E)\bar{G}_S^-(E) - \bar{G}_S^+(E)\hat{\Sigma}^<(E)]\,\mathrm{d}E \end{aligned} \tag{42}$$

$$\bar{G}_S^\pm(E) = (E\hat{1}_S - \hat{H}_{S_0} - \hat{\Sigma}^\pm \pm \mathrm{i}\hat{1}_S\Delta)^{-1}. \tag{43}$$

The screening of an extra scattering potential $\hat{v}$, provided by Δ, may be seen in the energy domain as follows. The full injection terms in the steady state, in the presence of the thermal broadening Δ, contain the full Green's function $\hat{G}_S^\pm(E) = (E\hat{1}_S - \hat{H}_{S_0} - \hat{v} - \hat{\Sigma}^\pm \pm \mathrm{i}\hat{1}_S\Delta)^{-1}$. Writing $\hat{G}_S^\pm(E)\hat{\Sigma}^<(E) = \bar{G}_S^\pm(E)\hat{\Sigma}^<(E) + \hat{G}_S^\pm(E)\hat{v}\bar{G}_S^\pm(E)\hat{\Sigma}^<(E)$, provided the distance between $L(R)$ and the scatterer is greater than $\sim v_\mathrm{e}\tau_\Delta$, the second term vanishes, because Δ makes $\bar{G}_S^\pm(E)$ exponentially small over that distance, and we rigorously recover (42).

For the model applications in this paper, we have made two simplifications to (42). First, we have set $\Delta = \Gamma/2$, so we have a single parameter to vary. Second, we have dropped $\hat{\Sigma}^\pm$ in $\bar{G}_S^\pm(E)$ in the injection terms in (42). This is formally correct to lowest order in the SP coupling, and simplifies the construction of the injection terms. This approximation may be extended beyond the limit of weak SP coupling under the following conditions. The neglect of $\hat{\Sigma}^\pm$ in $\bar{G}_S^\pm(E)$ is equivalent to replacing $\hat{W}_{S_0}(t,\tau)$ in the first term in (41) by the free propagator $\hat{U}_{S_0}(t,\tau) = \mathrm{e}^{-\mathrm{i}\hat{H}_{S_0}(t-\tau)/\hbar}$ in S, in the absence of $\hat{v}$ and in the absence of the probes. This retains single electron injection processes and excludes those corrections to the injection terms that arise from multiple coherent SP excursions. These higher-order corrections develop over times

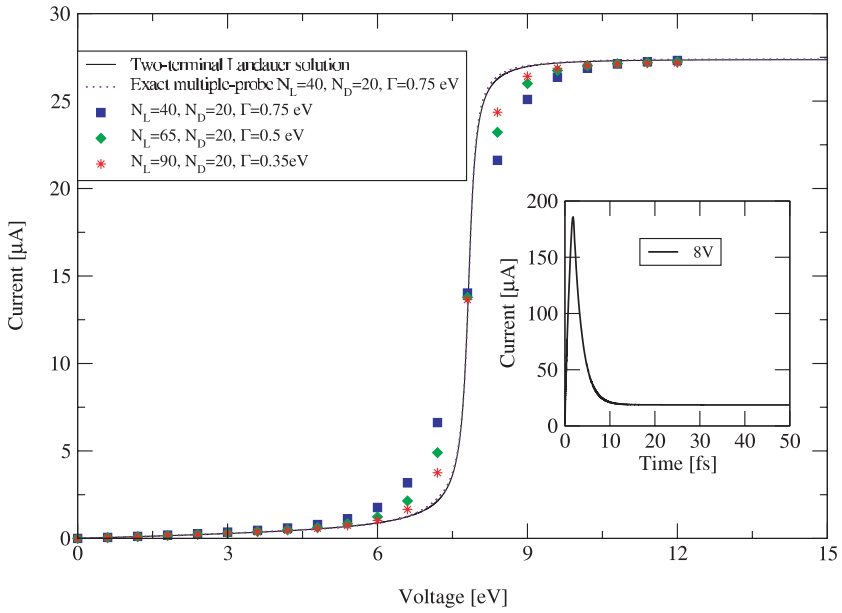

Figure 5. I–V curves for a resonant dimer obtained with the approximate time-dependent open boundaries in equation (44), compared with the unapproximated multiple-probe steady state from (2) and with the Landauer steady state. A typical current trace is shown in the inset ($N_L = 90$, $N_D = 20$, $\Gamma = 0.35$ eV, $V = 8$ V).

of the order of, or greater than, the mean electron residence time $\sim\hbar/\Gamma$ (from equation (12)) in the electrodes, in the presence of the probes. The dephasing factor in (41), on the other hand, restricts the memory of the injected intensity (modulus of amplitude, squared) to times $\sim\tau_\Delta/2 = \hbar/2\Delta$. Therefore, provided Δ is of the order of, or greater than, $\Gamma/2$, the contribution of multiple SP excursions to the injection terms is suppressed.

With these simplifications in place, the OB equation of motion reads

$$\mathrm{i}\hbar\,\dot{\hat{\rho}}_S(t) = [\hat{H}_S(t), \hat{\rho}_S(t)] + \hat{\Sigma}^+\hat{\rho}_S(t) - \hat{\rho}_S(t)\hat{\Sigma}^- + \int_{-\infty}^{+\infty} [\hat{\Sigma}^<(E)\tilde{G}_S^-(E) - \tilde{G}_S^+(E)\hat{\Sigma}^<(E)]\,\mathrm{d}E \tag{44}$$

$$\tilde{G}_S^\pm(E) = (E\hat{1}_S - \hat{H}_{S_0} \pm \mathrm{i}\hat{1}_S\Gamma/2)^{-1} \tag{45}$$

with $\hat{\Sigma}^\pm$ and $\hat{\Sigma}^<(E)$ given by equations (13) and (15). In the calculations below, the energy integral in (44) uses a lower limit chosen deep below the lower band edge for the system S. Calculations with the more elaborate form in (42) are left for future work.

The key limitation of (44) is that it gives a steady-state electronic structure with an energy broadening $\sim\Gamma$ (corresponding to 2Δ in the more general result in (42)). This is illustrated by applying (44) to a resonant dimer similar to that considered above. Figure 5 compares the steady-state I–V curves generated by (44) with the exact multiple-probe steady state from (2) and with the two-terminal Landauer steady state. As before, the system consists of two one-dimensional electrodes, each with N_L atoms, with a device region consisting of a chain of $N_D/2$ atoms on each side of the dimer. In this example, $t_{\mathrm{chain}} = -3.88$ eV, $t_{c-d} = -0.5$ eV and $t_{\mathrm{dimer}} = -3.88$ eV, with all onsite energies equal to zero, leading to a very narrow resonance. The values of current from the time-dependent simulation (given by the expectation of the tight-binding bond-current operator [26] in the instantaneous density matrix, in a bond chosen

somewhere between an electrode and the dimer) are obtained by integrating (44) until a steady state is reached (see the inset in the figure). The OB driving terms are switched on over a period of 5 fs at the start of the simulation and maintained thereafter. The unapproximated multiple-probe steady state from (2) is in excellent agreement with the two-terminal Landauer solution as expected. Equation (44) captures the resonance with an additional broadening that dies out with decreasing Γ. Decreasing Γ further still, so that the broadening is negligible, requires longer and longer leads (from (17)), for which the computation becomes impractical. However, this limitation is an artefact of the simplification in (44), which ties up the resolution-limiting parameter Δ with the lead-length-limiting parameter Γ. This restriction will, we hope, be lifted in future work based on (42), where the resolution-limiting parameter Δ (needed to screen out dynamical scattering in C) is set solely by the device length.

4. Application to correlated electron–ion dynamics (CEID)

In this section the approximate OB scheme in equation (44) is combined with the second-order CEID expansion in [21] and is applied to two model problems.

4.1. CEID equations of motion

The method for CEID in [21] is an expansion of the equation of motion for the many-body DM for a system of electrons and ions to first order in the correlated electron–ion fluctuations and to second order in ionic fluctuations about the mean ionic trajectory. The resultant system of equations of motion, for a set of electron–ion correlation functions, is then reduced to one-electron form by an extension of the Hartree–Fock approximation for the two-electron DM to take account of the spread of electronic trajectories, and resultant non-idempotency of the one-electron DM, to lowest order in the electron–ion correlations. This procedure yields the following equations of motion, given here for non-interacting electrons and one ionic dynamical degree of freedom,

$$\dot{\bar{R}} = \frac{\bar{P}}{M}, \qquad \dot{\bar{P}} = \bar{F}, \qquad \bar{F} = F_I + \mathrm{Tr}\{\hat{\rho}\hat{F}\} - \mathrm{Tr}\{\hat{\mu}\hat{K}\} \tag{46}$$

$$\dot{\hat{\rho}} = \frac{1}{\mathrm{i}\hbar}[\hat{H}, \hat{\rho}] - \frac{1}{\mathrm{i}\hbar}[\hat{F}, \hat{\mu}] + \frac{1}{2\mathrm{i}\hbar} C_{RR}[\hat{K}, \hat{\rho}] \tag{47}$$

$$\dot{\hat{\mu}} = \frac{1}{\mathrm{i}\hbar}[\hat{H}, \hat{\mu}] + \frac{\hat{\lambda}}{M} - \frac{1}{\mathrm{i}\hbar} C_{RR}[\hat{F}, \hat{\rho}] \tag{48}$$

$$\begin{aligned}\dot{\hat{\lambda}} = {} & \frac{1}{\mathrm{i}\hbar}[\hat{H}, \hat{\lambda}] - \frac{1}{\mathrm{i}\hbar} C_{RP}[\hat{F}, \hat{\rho}] + \frac{1}{2}(\hat{F}\hat{\rho} + \hat{\rho}\hat{F}) - \hat{\rho}\hat{F}\hat{\rho} + C_{RR}^{-1}(\hat{\mu}\,\mathrm{Tr}\{\hat{F}\hat{\mu}\} - \hat{\mu}\hat{F}\hat{\mu}) \\ & - \bar{K}\hat{\mu} - \tfrac{1}{2}(\hat{K}\hat{\mu} + \hat{\mu}\hat{K}) + (\hat{\mu}\hat{K}\hat{\rho} + \hat{\rho}\hat{K}\hat{\mu}), \qquad \bar{K} = K_I + \mathrm{Tr}\{\hat{K}\hat{\rho}\}\end{aligned} \tag{49}$$

$$\dot{C}_{RR} = \frac{2}{M} C_{RP}, \qquad \dot{C}_{RP} = \frac{C_{PP}}{M} + \mathrm{Tr}\{\hat{\mu}\hat{F}\} - \bar{K} C_{RR}, \qquad \dot{C}_{PP} = 2\,\mathrm{Tr}\{\hat{\lambda}\hat{F}\} - 2\bar{K} C_{RP}. \tag{50}$$

Above, $\hat{H} = \hat{H}(\bar{R})$ is the one-electron Hamiltonian in the presence of the ions, and we have introduced the force and stiffness operators

$$\hat{F} = \hat{F}(\bar{R}) = -\frac{\partial \hat{H}(\bar{R})}{\partial \bar{R}}, \qquad \hat{K} = \hat{K}(\bar{R}) = \frac{\partial^2 \hat{H}(\bar{R})}{\partial \bar{R}^2}$$

$$F_I = F_I(\bar{R}) = -\frac{\partial H_I(\bar{R})}{\partial \bar{R}}, \qquad K_I = K_I(\bar{R}) = \frac{\partial^2 H_I(\bar{R})}{\partial \bar{R}^2}$$

where H_I is the ion–ion interaction potential. M is the ionic mass. The one-electron DM is defined by $\hat{\rho} = \hat{\rho}(t) = N_e \mathrm{Tr}_{e,2\ldots N_e} \mathrm{Tr}_I\{\hat{\rho}_{eI}\}$ where $\hat{\rho}_{eI} = \hat{\rho}_{eI}(t)$ is the many-body DM for the whole system, including electrons and ions. We have also introduced the one-electron operators $\hat{\mu} = \hat{\mu}(t) = N_e \mathrm{Tr}_{e,2\ldots N_e} \mathrm{Tr}_I\{\Delta\hat{R}\hat{\rho}_{eI}\}$ and $\hat{\lambda} = \hat{\lambda}(t) = N_e \mathrm{Tr}_{e,2\ldots N_e} \mathrm{Tr}_I\{\Delta\hat{P}\hat{\rho}_{eI}\}$ which contain correlations between the electrons and ionic position and momentum, respectively. Here $\hat{R}$ and $\hat{P}$ are the ionic position and momentum operators and $\Delta\hat{R} = \hat{R} - \bar{R}$, $\bar{R} = \bar{R}(t) = \mathrm{Tr}_{e,I}\{\hat{R}\hat{\rho}_{eI}\}$, $\Delta\hat{P} = \hat{P} - \bar{P}$, $\bar{P} = \bar{P}(t) = \mathrm{Tr}_{e,I}\{\hat{P}\hat{\rho}_{eI}\}$. The quantities $C_{RR} = C_{RR}(t) = \mathrm{Tr}_{e,I}\{(\Delta\hat{R})^2\hat{\rho}_{eI}\}$, $C_{RP} = C_{RP}(t) = \mathrm{Tr}_{e,I}\{(\Delta\hat{R}\Delta\hat{P} + \Delta\hat{P}\Delta\hat{R})\hat{\rho}_{eI}\}/2$, $C_{PP} = C_{PP}(t) = \mathrm{Tr}_{e,I}\{(\Delta\hat{P})^2\hat{\rho}_{eI}\}$ are the widths of the ionic phase-space distribution and measure the effective degree of vibrational excitation of the ion.

Equations (46)–(50) can be viewed as low-order corrections to Ehrenfest dynamics. Ehrenfest dynamics arises in the limit of vanishing electron–ion correlations ($\hat{\mu} = 0$, $\hat{\lambda} = 0$) and vanishing ionic fluctuations ($C_{RR} = 0$, $C_{RP} = 0$, $C_{PP} = 0$), when equations (46)–(50) reduce to

$$\dot{\bar{R}} = \frac{\bar{P}}{M}, \qquad \dot{\bar{P}} = \bar{F}, \qquad \bar{F} = F_I + \mathrm{Tr}\{\hat{\rho}\hat{F}(\bar{R})\}, \qquad \dot{\hat{\rho}} = \frac{1}{\mathrm{i}\hbar}[\hat{H}(\bar{R}), \hat{\rho}]. \tag{51}$$

Equations (46)–(50) then reinstate various corrections to Ehrenfest dynamics. For example, the terms $(\hat{F}\hat{\rho} + \hat{\rho}\hat{F})/2 - \hat{\rho}\hat{F}\hat{\rho}$ in (49) nucleate inelastic electron–ion scattering, in a way that accommodates the fermionic statistics of the electrons. The term $-C_{RR}[\hat{F}, \hat{\rho}]/\mathrm{i}\hbar$ in (48) introduces the inelastic scattering cross-section of the vibrating ion, C_{RR}, that electrons see. The term $-[\hat{F}, \hat{\mu}]/\mathrm{i}\hbar$ has the job of collecting this information and depositing it in (47), so as to generate effective corrections to the electron propagation, and the redistribution of electrons in energy, caused by the inelastic scattering with ions. Power is injected into ionic vibrations by the term $\mathrm{Tr}\{\hat{\lambda}\hat{F}\}$ in $\dot{C}_{PP}$ in (50), which contains the correlated force–momentum fluctuations, required for energy transfer.

The CEID equations have a relation to scattering theory. When applied to a harmonic oscillator linearly coupled to electrons in an infinite wire, to lowest order in the electron–oscillator coupling $\hat{F}$, (46)–(50) analytically return the scattering rates from the Fermi Golden Rule (FGR) [21]

$$\begin{aligned}\dot{f}_\alpha = \frac{2\pi}{\hbar}\frac{\hbar}{2M\omega}\sum_\beta |F_{\alpha\beta}|^2\{&-(N+1)f_\alpha(1-f_\beta)\delta(E_{\beta\alpha}+\hbar\omega) - Nf_\alpha(1-f_\beta)\delta(E_{\beta\alpha}-\hbar\omega)\\ &+ (N+1)f_\beta(1-f_\alpha)\delta(E_{\beta\alpha}-\hbar\omega) + Nf_\beta(1-f_\alpha)\delta(E_{\beta\alpha}+\hbar\omega)\}\end{aligned} \tag{52}$$

where α labels the eigenstates, with energies $\{E_\alpha\}$ and occupancies $\{f_\alpha\}$, of the one-electron Hamiltonian in the absence of the oscillator, $E_{\beta\alpha} = E_\beta - E_\alpha$, ω is the angular frequency of the oscillator and N is the effective number of quanta of excitation of the oscillator, related to the CEID variable C_{RR} through $M\omega^2 C_{RR} = (N + 1/2)\hbar\omega$. At the same time, (46)–(50) go beyond the FGR, in that, when integrated together, they sum these lowest-order scattering processes to higher orders in $\hat{F}$, in distinct similarity to the self-consistent Born approximation (SCBA) (a recent survey of these methods is given in [28]). A difference from conventional scattering theory is that, when used with an explicit electron–ion interaction Hamiltonian, (46)–(50) do not pre-calculate oscillator normal modes and frequencies as an input, but generate them in the course of the solution [21]. A further difference, at least of form, is that CEID uses instantaneous variables interpretable in MD terms.

Equation (52) captures the spontaneous emission of phonons by excited electrons, responsible for the inelastic corrections to I–V spectra at low temperatures and for ionic heating under current flow. Therefore, we expect the CEID equations (46)–(50) to be able to capture these processes also.

4.2. CEID with open boundaries

Equations (47)–(49) may be written as

$$\mathrm{i}\hbar\,\dot{\hat{q}} = [\hat{H}, \hat{q}] + \hat{\Lambda}^{(q)}, \qquad \hat{q} = \hat{\rho}, \hat{\mu}, \hat{\lambda} \tag{53}$$

where $\hat{\Lambda}^{(q)}$ describe electron–ion dynamical scattering. To apply the approximate OB result in equation (44), we imagine that the dynamical ionic degrees of freedom are located in the interior of region C in figure 1 and we write the OB equations of motion in S

$$\mathrm{i}\hbar\,\dot{\hat{q}}_S = [\hat{H}_S, \hat{q}_S] + \hat{\Lambda}^{(q)}_S + \hat{D}^{(q)}, \qquad \hat{q} = \hat{\rho},\ \hat{\mu},\ \hat{\lambda} \tag{54}$$

$$\hat{D}^{(\rho)} = \hat{\Sigma}^{+}\hat{\rho}_S - \hat{\rho}_S\hat{\Sigma}^{-} + \int_{-\infty}^{+\infty} [\hat{\Sigma}^{<}(E)\tilde{G}^{-}_S(E) - \tilde{G}^{+}_S(E)\hat{\Sigma}^{<}(E)]\,\mathrm{d}E \tag{55}$$

$$\hat{D}^{(\mu)} = \hat{\Sigma}^{+}\hat{\mu}_S - \hat{\mu}_S\hat{\Sigma}^{-}, \qquad \hat{D}^{(\lambda)} = \hat{\Sigma}^{+}\hat{\lambda}_S - \hat{\lambda}_S\hat{\Sigma}^{-} \tag{56}$$

where for the last two equations we have used the analogues to (19) $\hat{\mu}_P(0) = 0$, $\hat{\lambda}_P(0) = 0$. Following section 3.2, the Hamiltonian $\hat{H}_{S_0}$ to be used in the construction of $\tilde{G}^{\pm}_S(E)$ in (55) is taken as the electronic Hamiltonian evaluated at the classical ionic positions at $t = 0$.

To summarize: at the present level of approximation, (i) the injection Green's functions $\tilde{G}^{\pm}_S(E)$ for $\hat{\rho}_S$ carry an extra $\pm\hat{1}_C\Gamma/2$ (or $\pm\hat{1}_S\Delta$ in the more elaborate result in (42)) which masks the CEID scattering potential in C at the cost of introducing an effective thermal broadening $\sim\Gamma$ (2Δ in (42)) in the incoming electronic distributions; (ii) the injection Green's function is missing a self-energy to account for the coherent addition of injection and subsequent scattering that builds up in time; (iii) the electron–ion correlation operators $\hat{\mu}_S$ and $\hat{\lambda}_S$ have no injection terms. Items (ii) and (iii) in the presence of (i) are justified for a long enough device. The removal of (i)–(iii), so as to remove the artificial energy broadening and reinstate the coherence between injection and CEID scattering in C, is a subject for future work.

4.3. A benchmark calculation: inelastic I–V characteristics in a closed system

To provide a basis for comparison with the OB CEID simulations, we first revisit a calculation in [21]. In this calculation, (46)–(50) are applied to current flow in a finite closed system (without OB driving terms) and are used to extract the resultant inelastic I–V spectrum. The system is an atomic chain containing a single dynamical quantum ion of mass $M = 1$ amu at the centre of the chain. Only longitudinal motion of the ion is allowed at present. Electron–ion interactions are described through a single-orbital tight-binding model, and ion–ion interactions through a repulsive pair potential, with parameters fitted to the elastic properties of bulk gold [29]. In the present calculations, the band filling is 1/2. The bond length in the chain is 2.5 Å. As in [21], initially a static bias V is applied across the middle of the chain, the ground-state electronic DM in the presence of this bias is found, after which the bias is removed, over a period of 5 fs, resulting in a flow of current.

Here, we make two modifications compared with [21] to enable a more detailed comparison with scattering theory. In [21], the ion was allowed to heat up in the course of the simulation. By contrast, here we keep C_{RR}, C_{RP} and C_{PP} fixed at their initial values, set to those for the vibrational ground state of the dynamical ion in the Born–Oppenheimer approximation. This corresponds to setting $N = 0$, $\omega = \omega_{\mathrm{BO}}$ in the FGR, where ω_{BO} is the Born–Oppenheimer angular frequency of the ion. For the present parameters, $\hbar\omega_{\mathrm{BO}} = 0.26$ eV. $\bar{R}$ is held fixed at the equilibrium ionic position and $\bar{P}$ is held fixed at zero. This procedure corresponds, notionally, to connecting the dynamical ion to an infinitely efficient external thermostat at zero temperature. This procedure retains the inelastic I–V corrections

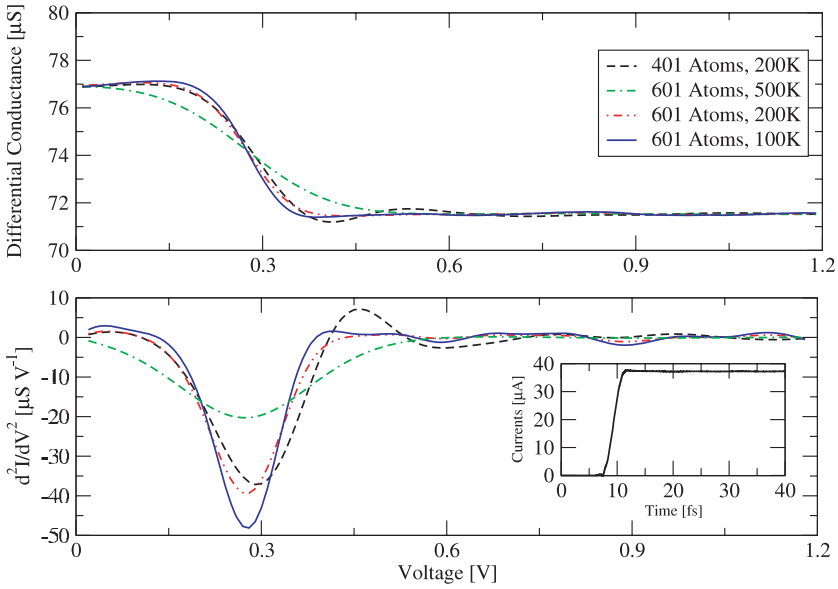

Figure 6. Differential conductance and its derivative with respect to voltage for an atomic chain with one dynamical ion of mass 1 amu, for different chain lengths and electronic temperatures. A current trace for a 601-atom chain at $T_e = 100$ K, for $V = 0.5$ V is shown in the inset. The Born–Oppenheimer angular frequency for the ion is $\hbar\omega_{BO} = 0.26$ eV.

due to spontaneous phonon emission at zero temperature and eliminates the additional I–V corrections due to actual variations in the effective ionic energy [30]. Here, furthermore, we consider a range of electronic temperatures T_e, which enter the calculation in the construction of the initial electronic DM. We then integrate equations (47)–(49) with $\hat{\mu}(0) = 0$, $\hat{\lambda}(0) = 0$ and take an I–V spectrum by averaging the current over a 25 fs time interval following the removal of the external bias. The results are shown in figure 6 and may be understood with the help of the FGR as follows.

Consider for a moment a lead–sample–lead system in the Landauer picture. The one-electron stationary states in the absence of phonons are Lippmann–Schwinger scattering states, derived from incident waves in the left and right lead and populated with electrochemical potentials offset by the bias eV [26]. For a ballistic conductor these states are pure Bloch waves and the FGR scattering rates between waves of opposite velocity directly give the inelastically backscattered electron current [31][10]. At zero electronic temperature, the differential conductance for an Einstein oscillator of angular frequency ω, in the vibrational ground state, in a perfect wire is given by

$$\frac{\mathrm{d}I}{\mathrm{d}V} = G_{\mathrm{el}} - G_0\,\theta(|eV| - \hbar\omega)\,4\pi^2\frac{\hbar}{2M\omega}\,T_{12} = G_0 - G_0\,\theta(|eV| - \hbar\omega)\,4C_{RR}\left(\frac{H'}{H}\right)^2 \qquad (57)$$

with $C_{RR} = (N + 1/2)\hbar/M\omega$, $\omega = \omega_{BO}$, $N = 0$. Above, G_{el} is the zero-bias elastic (phonon-free) conductance, $\theta(x)$ is the Heaviside step function and $T_{12} = \mathrm{Tr}[\hat{D}_1(E_F)\hat{F}\hat{D}_2(E_F)\hat{F}]$, where $\hat{D}_{1(2)}(E_F)$ are the partial density of states operators for the two classes of electronic states above, evaluated at the Fermi level E_F. To derive (57) from (52), we have ignored

[10] This result needs to be modified if there is non-zero elastic backscattering in the absence of phonons, when the Lippmann–Schwinger reference states already contain a mixture of Bloch waves [31, 32].

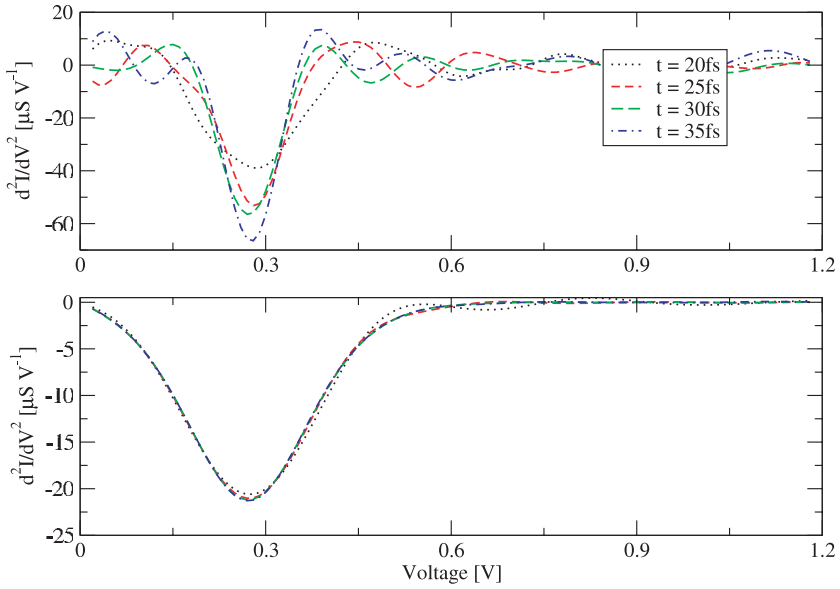

Figure 7. $\mathrm{d}^2I/\mathrm{d}V^2$ for a dynamical ion in a 601-atom chain, at $T_\mathrm{e} = 100$ K (upper plot) and $T_\mathrm{e} = 500$ K (lower plot). The current was averaged over a series of 5 fs time windows, whose initial time is the label for each curve.

variations of $\hat{D}_{1(2)}(E)$ over energy intervals of the order of $|eV|$ or $\hbar\omega$ near E_F. The second result in (57) is for a linear chain in a nearest-neighbour tight-binding model, with a hopping integral H with derivative with distance H'. The inelastic suppression of the conductance is a step-function of bias at $|eV| = \hbar\omega$, with a magnitude $0.082\,G_0$ for the present parameters. At non-zero electronic temperature, T_e, the Fermi–Dirac occupancies $\{f_\alpha\}$ in (52) are no longer step functions of energy and the step function in (57) broadens into a function with a derivative with a characteristic width $\Delta E_{T_\mathrm{e}} \sim 5.4k_\mathrm{B}T_\mathrm{e}$ [30, 33].

The CEID simulation in figure 6 captures several features of this behaviour. The position and magnitude of the inelastic drop in conductance agree well with the expected values, while decreasing T_e leads to a significant sharpening of the I–V feature. The width at $T_\mathrm{e} = 100$ K is considerably smaller than that observed in [21], where T_e was 500 K.

The improvement in resolution with decreasing T_e in the present calculations is limited by two factors. One is the finite energy-level spacing (∼0.04 eV at the Fermi level for the 601-atom chain). The other is the finite time of propagation of the dynamical equations, t. The energy-conserving delta functions in (52) emerge in the limit $t \to \infty$, while at finite times scattering rates retain an energy width $\Delta E_t \propto \hbar/t$. One of the findings of [21], for $T_\mathrm{e} = 500$ K, was that the width of the inelastic feature did not decrease with increasing time of propagation. By contrast, at the much lower electronic temperature $T_\mathrm{e} = 100$ K in figure 7 (upper panel) we see a marked improvement in resolution with increasing t. For $T_\mathrm{e} = 500$ K (lower panel), ΔE_t is masked by ΔE_{T_e}, and the resolution becomes independent of t, as in [21]. The above observations illustrate the agreement between CEID and scattering theory. We conclude that the resolution of inelastic I–V spectra in [21] was limited by T_e rather than by an intrinsic broadening of the electron and vibrational band structure generated by equations (46)–(50), and that any such intrinsic broadening is below the resolution of the present calculations.

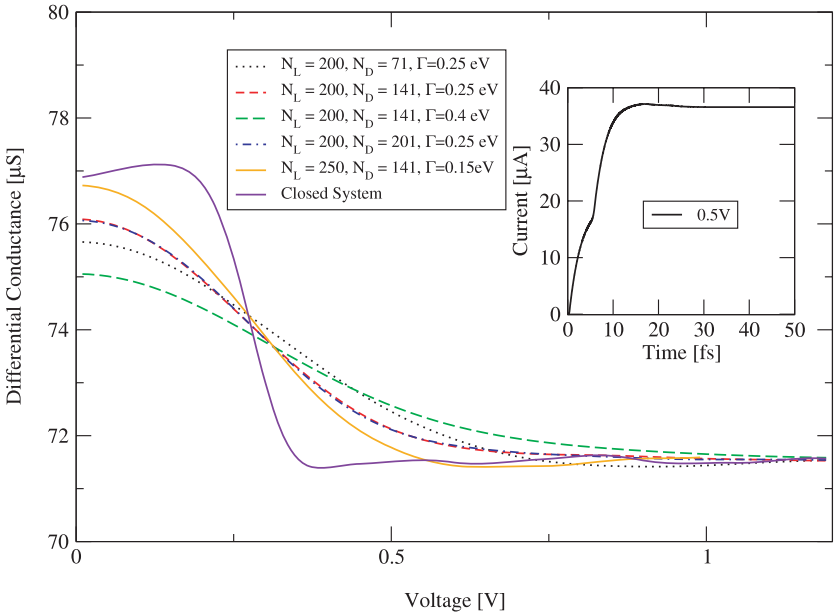

Figure 8. Differential conductance for a dynamical ion in an atomic wire, using the open-boundary formalism, for various system lengths and electrode–probe coupling strengths. Also shown is the differential conductance from the benchmark closed-system simulation. The inset shows a typical current trace ($N_L = 200$, $N_D = 141$, $\Gamma = 0.25$ eV, $V = 0.5$ V).

4.4. CEID with open boundaries: inelastic I–V spectra

The OB CEID equations of motion (54)–(56) are now used to generate steady-state currents and a corresponding I–V spectrum for a dynamical quantum ion in a chain with the same tight-binding parameters and ionic mass as above. The electronic temperature used in the injection terms in equations (44) and (55) is zero. The ionic variables $\bar{R}$, $\bar{P}$, C_{RR}, C_{RP} and C_{PP} are held frozen at the values for the Born–Oppenheimer vibrational ground state as in section 4.3.

Figure 8 shows the results for different lengths of the device region (region C in figure 1, with the dynamical ion at the centre), different lead lengths (regions L and R) and different values of the parameter Γ, and compares them with the earlier closed-system calculation for a 601-atom chain and $T_e = 100$ K. The inelastic I–V feature in the OB steady state is present, but is broadened. The sharpness of the feature saturates with device length, and is limited by Γ. This is the expected error, due to the energy broadening introduced by the approximate injection terms in (55) and (56). As Γ decreases, the resolution improves and the magnitude of the inelastic drop in conductance agrees more and more closely with the expected values from the closed-system calculation and from scattering theory.

4.5. Ionic heating and equilibration

Having propagated equations (54)–(56) with frozen ionic variables ($\bar{R}$, $\bar{P}$, C_{RR}, C_{RP} and C_{PP}) to a steady state as in the previous subsection, the ionic variables are now unfrozen and are allowed to propagate according to equations (46), (50). Figures 9 and 10 show the total ionic energy[11] and the current in the wire as a function of time for two different ionic masses. The

[11] Following [21], the total ionic energy plotted here is taken as $(C_{PP}/2M + K_{BO}C_{RR}/2)$. This is the quantity used in scattering calculations of heating, for example. $K_{BO} \sim 260$ J m^{-2} is the Born–Oppenheimer stiffness for the oscillator.

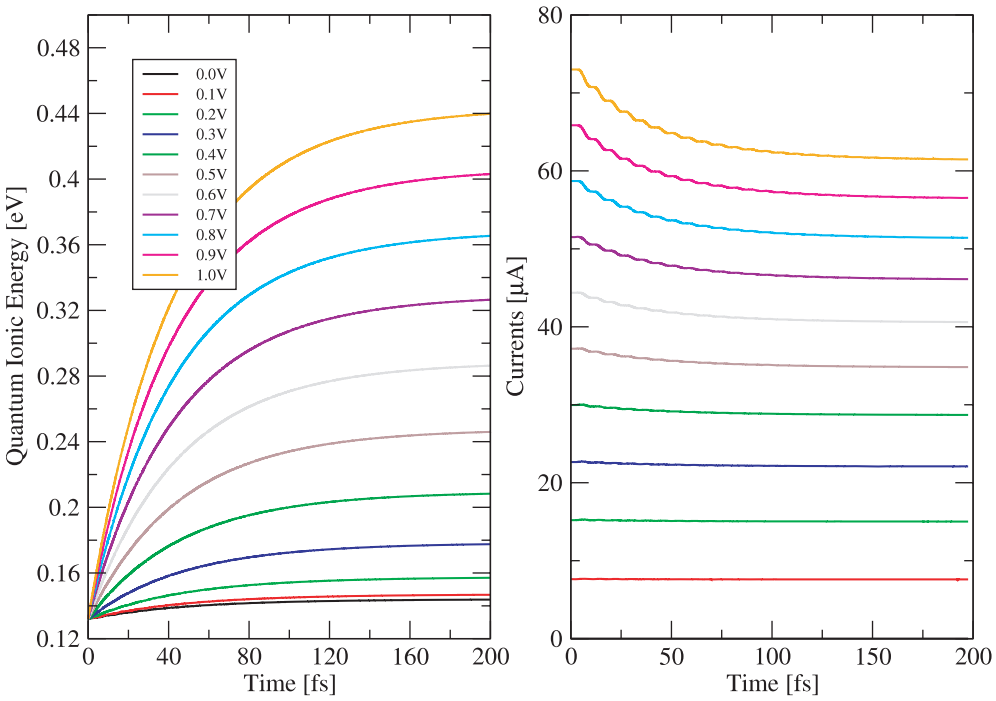

Figure 9. Vibrational energy of a single dynamical ion with $M = 1$ amu at various voltages, with corresponding currents. $N_L = 200$, $N_D = 201$, $\Gamma = 0.2$ eV. Curves from bottom to top correspond to voltages from 0 to 1 V.

ion heats up in time to a bias-dependent asymptotic value, while the current decreases in the course of the ionic heating. The heating rate depends on the ionic mass but the asymptotic values of the ionic energy and current, for a given bias, are approximately independent of mass.

To understand these results, we return to the FGR. For the power into an Einstein oscillator in a current-carrying wire, at zero electronic temperature, in the Landauer picture, (52) gives [19, 31]

$$\dot{E} = \frac{2\pi\hbar}{M}\,[-E(T_{11} + 2T_{12} + T_{22}) + (|eV| - \hbar\omega)\theta(|eV| - \hbar\omega)\,T_{12}], \qquad E = N\hbar\omega \quad (58)$$

where $T_{ij} = \mathrm{Tr}[\hat{D}_i(E_\mathrm{F})\hat{F}\hat{D}_j(E_\mathrm{F})\hat{F}]$ and, as in (57), we have ignored variations of $\hat{D}_{1(2)}(E)$ over energy intervals of the order of $|eV|$ or $\hbar\omega$ near E_F. This result may be extended to more than one vibrational degree of freedom [31]. The power into vibrational modes in atomic wires has also been calculated within NEGF and extended to non-zero electronic temperature [32, 34, 35]. In the absence of lattice heat conduction away from the oscillator, setting $\dot{E} = 0$ in (58) gives the oscillator energy, $E = E_\infty$, that the oscillator needs, in order to be in equilibrium with the current-carrying electrons [31, 35, 36]. For $|eV| > \hbar\omega$, the result is

$$U_\infty = E_\infty + \frac{\hbar\omega}{2} = \frac{\hbar\omega}{2} + \frac{T_{12}}{T_{11} + 2T_{12} + T_{22}}\,(|eV| - \hbar\omega) \leqslant \frac{\hbar\omega}{2} + \frac{1}{2}\,(|eV| - \hbar\omega) = \frac{|eV|}{2}. \quad (59)$$

If expressed in terms of a notional oscillator temperature T_∞ via $U_\infty = (N_\infty + 1/2)\hbar\omega$, $N_\infty = 1/(\mathrm{e}^{\hbar\omega/k_\mathrm{B}T_\infty} - 1)$, (59) reads $k_\mathrm{B}T_\infty \leqslant |eV|/2$. Equality in (59) is achieved for $T_{11} = T_{22} = 0$. This is the case for an Einstein oscillator in a chain in the present tight-binding model,

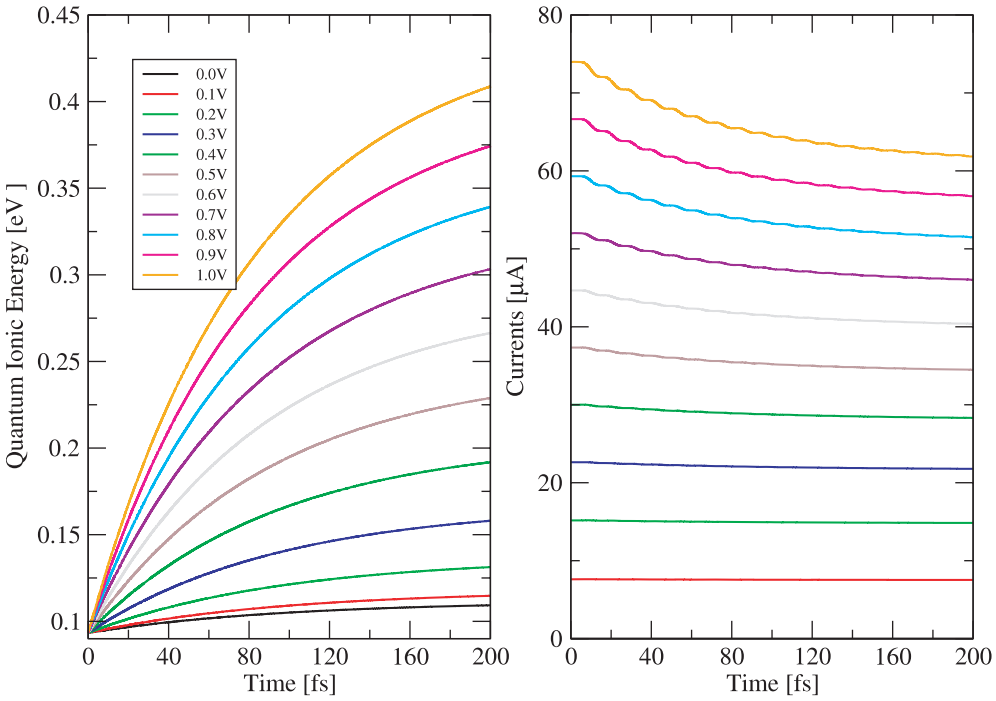

Figure 10. Vibrational energy of a single dynamical ion with $M = 2$ amu at various voltages, with corresponding currents. $N_L = 200$, $N_D = 201$, $\Gamma = 0.2$ eV.

when (58) becomes [19] $\dot{E} = (2\pi\hbar/M)(1/\pi^2)\,[-2E+(|eV|-\hbar\omega)\theta(|eV|-\hbar\omega)](H'/H)^2$. If we think of this as a rate equation [32], then for the oscillator energy $U = U(t) = \hbar\omega/2+E(t)$, with $U(0) = \hbar\omega/2$, we get

$$U(t) = \frac{1}{2}\hbar\omega + \frac{1}{2}(1 - \mathrm{e}^{-t/\tau})(|eV| - \hbar\omega)\theta(|eV| - \hbar\omega)], \qquad \frac{1}{\tau} = \frac{4\pi\hbar}{M}\frac{1}{\pi^2}\left(\frac{H'}{H}\right)^2. \quad (60)$$

For our quantum ion, therefore, the FGR predicts heating, with a rate $1/\tau$, towards an asymptotic value $U_\infty = |eV|/2$.

The results of the OB CEID simulations in figures 9 and 10 agree closely with these expectations. To quantify the comparison, a fit is made to the heating data using the functional form in (60), with ω set to ω_{BO} in the first term and with the prefactor and τ in the second term as adjustable parameters in the fit. The fit gives $\tau \sim 47$ fs for $M = 1$ amu at the inelastic threshold compared with an expected value of $\tau = 48$ fs from (60) for the present parameters. For $M = 2$ amu the fit gives $\tau \sim 95$ fs against an expected value of $\tau = 96$ fs. The fitted values of τ show some variation ($\sim$10%) over the range of biases in the figure. A small amount of ionic heating observed below the inelastic threshold reflects the broadening of the incoming electronic distributions by the parameter Γ in the time-dependent OB simulations.

These results are summarized in figure 11 which shows the asymptotic value of the ionic energy as a function of bias, obtained by extrapolating the result from the fit to infinite times. The above results for the maximal heating of a vibration in a metallic wire, in the absence of cooling by lattice heat conduction, agree with the results reported in [30], and are significantly lower than those reported in [37, 38].

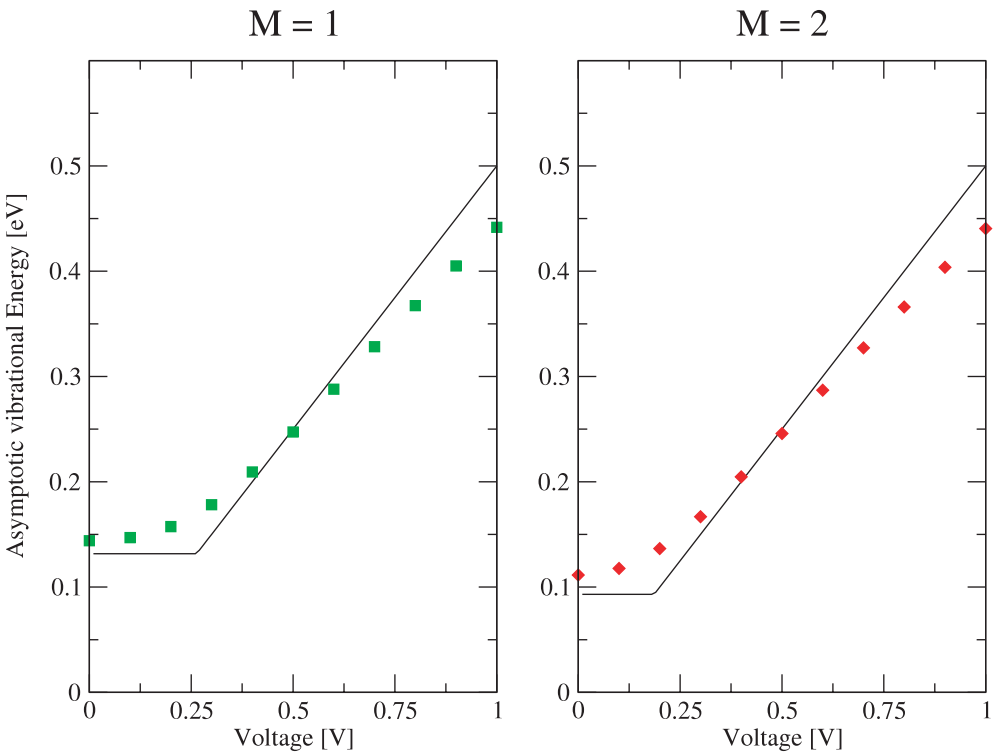

Figure 11. Extrapolated ($t \to \infty$) maximal vibrational energy of a single dynamical ion of mass M in a 601-atom chain, for $M = 1$ amu (left) and $M = 2$ amu (right). The solid line is the result from the Fermi golden rule at zero temperature; the points are from the open-boundary CEID simulations. Details are in the text.

The decrease in current with time in figures 9 and 10 is due to the increase in scattering cross-section, C_{RR}, with ionic heating. The maximal vibrational energy of the ion, $U(\infty) \approx |eV|/2$, is set by the bias and is independent of ionic mass. If we assume equipartitioning between ionic kinetic energy ($C_{PP}/2M$) and potential energy ($K_{\mathrm{BO}}C_{RR}/2$), then, since K_{BO} is itself independent of ionic mass, we expect the maximal value of C_{RR} to be mass-independent, and hence the maximal reduction in current for a given bias to be mass-independent. This expectation is reasonably borne out by figures 9 and 10, where the asymptotic value of the current for a given bias is roughly the same for the two masses. This mass-independent maximal suppression of the current, therefore, probes directly the strength of the effective underlying electron–phonon scattering potential.

We may estimate the suppression in current analytically, to compare with the numerical results, as follows. Consider an ion rigidly displaced by an amount ΔR in an otherwise perfect tight-binding atomic chain. For the zero-bias conductance, at the band centre, the Landauer formula [26] gives $\mathrm{d}I/\mathrm{d}V = G_0\, 4\,\lambda_1^2\lambda_2^2/(\lambda_1^2+\lambda_2^2)^2$, where $\lambda_{1(2)} = H_{1(2)}/H$, with $H_{1(2)}$ the hopping integrals on either side of the displaced ion and H the equilibrium hopping integral. Writing $\lambda_{1(2)} \approx (1 \pm \delta)$, $\delta = H'\Delta R/H$, for the reduction in conductance below the ballistic value we have $\Delta\mathrm{d}I/\mathrm{d}V = G_0 - \mathrm{d}I/\mathrm{d}V \approx G_0\, 4\,\delta^2/(1+\delta^2)^2$. Setting $\Delta R^2 = C_{RR}$ gives $\delta^2 = C_{RR}(H'/H)^2$. From the value of C_{RR} at the end of the simulation (200 fs) for $M = 2$ amu and $V = 1$ V in figure 10, which is such that $K_{\mathrm{BO}}C_{RR}/2 \approx 0.21$ eV, we obtain $\delta^2 \approx 0.066$,

with $\Delta \mathrm{d}I/\mathrm{d}V \approx 0.23\,G_0$ and a total current $I \approx (G_0 - \Delta \mathrm{d}I/\mathrm{d}V)V \approx 59\ \mu$A, in reasonable agreement with the value in the figure.

5. Summary

A method for correlated electron–ion dynamics was combined with electronic OB and was applied to a model simulation of the heating of a quantum ion in a current-carrying atomic wire, the eventual equilibration of the ion with the current and the accompanying response of the current in real time. While the initial heating rate scales inversely with ionic mass, the eventual maximal ionic energy and corresponding maximal suppression of the current for a given bias are largely mass-independent, in agreement with the predictions of scattering theory. The maximal values of the suppression of the current directly probe the strength of the effective electron–phonon interaction potential $\hat{F}$. In the present simulations, no lattice heat conduction was taken into account. This case is not irrelevant since atomic-scale junctions can harbour highly localized vibrational modes, due to their topological inhomogeneity [31]. However, the inclusion of a thermostat for the quantum ions to model heat loss to the electrodes is an important extension for the future. The method furthermore enables the calculation of inelastic I–V corrections in the steady state, but at present can only do so with a limited resolution, due to the dephasing approximation in the electron injection terms.

While only a modest step in the development of MD simulations of current-carrying nanostructures, the present type of simulation introduces a key element: the heating of atomic vibrations under steady current, with both electrons and ions treated dynamically on an equal quantum-mechanical footing. However, much more work lies ahead on the road to the realistic simulation of current-driven dynamics in nanowires. For the present simulations directions for future improvement are: corrections to the OB injection terms to take account of the coherence between injection and subsequent scattering that builds up in time; introduction of lattice heat conduction into the environment; inclusion of electron–electron screening, at least at the level of the extended Hartree–Fock approximation proposed in [21]. It was noted earlier that the present form of the CEID bears suggestive similarities to SCBA. A formal comparison between the two is an attractive future study. Finally, the CEID expansion used here was derived in the limit of weak correlations between electrons and ionic vibrations. To address problems where this correlation is strong requires a re-formulation of the method. Work on this is under way.

Acknowledgments

This work is funded by EPSRC under grant no EP/C006739/01. DRB acknowledges the Royal Society for support through a University Research Fellowship. Discussions with P Delaney, J M van Ruitenbeek and A Sakai are gratefully acknowledged. This work made use of the facilities of HPCx, the UK's national high-performance computing service, provided by EPCC at the University of Edinburgh and by CCLRC Daresbury Laboratory, and funded by the Office of Science and Technology through EPSRC's High End Computing Programme.

References

[1] Agraït N, Yeyati A L and van Ruitenbeek J M 2003 *Phys. Rep.* **377** 81
[2] Todorov T N and Sutton A P 1993 *Phys. Rev. Lett.* **70** 2138
Todorov T N and Sutton A P 1996 *Phys. Rev.* B **54** R14234

[3] Brandbyge M, Schiotz J, Sorensen M R, Stoltze P, Jacobsen K W, Nosrkov J K, Olesen L, Laegsgaard E, Stensgaard I and Besenbacher F 1995 *Phys. Rev.* B **52** 8499
[4] Landman U, Luedtke W D, Salisbury B E and Whetten R L 1996 *Phys. Rev. Lett.* **77** 1362
[5] Sorensen M R, Brandbyge M and Jacobsen K W 1998 *Phys. Rev.* B **57** 3283
[6] Barnett R N and Landman U 1997 *Nature* **387** 788
[7] Taraschi G, Mozos J L, Wan C C, Guo H and Wang J 1998 *Phys. Rev.* B **58** 13138
[8] Nakamura A, Brandbyge M, Hansen L B and Jacobsen K W 1999 *Phys. Rev. Lett.* **82** 1538
[9] Di Ventra M, Pantelides S T and Lang N D 2002 *Phys. Rev. Lett.* **88** 046801
[10] Brandbyge M, Stokbro K, Taylor J, Mozos J-L and Ordejón P 2003 *Phys. Rev.* B **67** 193104
[11] Todorov T N, Hoekstra J and Sutton A P 2001 *Phys. Rev. Lett.* **86** 3606
[12] van den Brom H E, Yanson A I and van Ruitenbeek J M 1998 *Physica* B **252** 69
[13] Smit R H M, Untiedt C and van Ruitenbeek J M 2004 *Nanotechnology* **15** S472
[14] Tsutsui M, Kurokawa S and Sakai A 2006 *Nanotechnology* **17** 5334
[15] Agraït N, Untiedt C, Rubio-Bollinger G and Vieira S 2002 *Phys. Rev. Lett.* **88** 216803
[16] Itakura K, Yuki K, Kurokawa S, Yasuda H and Sakai A 1999 *Phys. Rev.* B **60** 11163
[17] Horsfield A P, Bowler D R and Fisher A J 2004 *J. Phys.: Condens. Matter* **16** L65
[18] Verdozzi C, Stefanucci G and Almbladh C-O 2006 *Phys. Rev. Lett.* **97** 046603
[19] Horsfield A P, Bowler D R, Fisher A J, Todorov T N and Montgomery M J 2004 *J. Phys.: Condens. Matter* **16** 3609
[20] Horsfield A P, Bowler D R, Fisher A J, Todorov T N and Sánchez C G 2004 *J. Phys.: Condens. Matter* **16** 8251
[21] Horsfield A P, Bowler D R, Fisher A J, Todorov T N and Sánchez C G 2005 *J. Phys.: Condens. Matter* **17** 4793
[22] Bowler D R, Horsfield A P, Sánchez C G and Todorov T N 2005 *J. Phys.: Condens. Matter* **17** 3985
[23] Sánchez C G, Stamenova M, Sanvito S, Bowler D R, Horsfield A P and Todorov T N 2006 *J. Chem. Phys.* **124** 214708
[24] Kurth S, Stefanucci G, Almbladh C-O, Rubio A and Gross E K U 2005 *Phys. Rev.* B **72** 035308
[25] Zhu Y, Maciejko J, Ji T, Guo H and Wang J 2005 *Phys. Rev.* B **71** 075317
[26] Todorov T N 2002 *J. Phys.: Condens. Matter* **14** 3049
[27] Meir Y and Wingreen N S 1992 *Phys. Rev. Lett.* **68** 2512
[28] Horsfield A P, Bowler D R, Ness H, Sánchez C G, Todorov T N and Fisher A J 2006 *Rep. Prog. Phys.* **69** 1195
[29] Sutton A P, Todorov T N, Cawkwell M J and Hoekstra J 2001 *Phil. Mag.* B **81** 1833
[30] Frederiksen T, Brandbyge M, Lorente N and Jauho A-P 2004 *Phys. Rev. Lett.* **93** 256601
[31] Montgomery M J, Hoekstra J, Todorov T N and Sutton A P 2003 *J. Phys.: Condens. Matter* **15** 731
Montgomery M J and Todorov T N 2003 *J. Phys.: Condens. Matter* **15** 8781
Montgomery M J and Todorov T N 2004 *J. Phys.: Condens. Matter* **16** 6819
[32] Paulsson M, Frederiksen T and Brandbyge M 2005 *Phys. Rev.* B **72** 201101
[33] Lambe J and Jaklevic R C 1968 *Phys. Rev.* **165** 821
[34] Viljas J K, Cuevas J C, Pauly F and Häfner M 2005 *Phys. Rev.* B **72** 245415
[35] Frederiksen T, Paulsson M, Brandbyge M and Jauho A-P 2007 *Phys. Rev.* B at press (*Preprint* cond-mat/0611562)
[36] Ralls K S, Ralph D C and Buhrman R A 1989 *Phys. Rev.* B **40** 11561
Holweg P A M, Caro J, Verbruggen A H and Radelaar S 1992 *Phys. Rev.* B **45** 9311
[37] Chen Y-C, Zwolak M and Di Ventra M 2003 *Nano Lett.* **3** 1691
[38] Yang Z, Chshiev M, Zwolak M, Chen Y-C and Di Ventra M 2005 *Phys. Rev.* B **71** 041402